Hybrid Organic-Inorganic Materials Comprising Zirconia, Silica, and Thiazole Dye by Sol-Gel Process

Chien-Wen Chen,[1] Mu-Cheng Kuo,[1] Jyh-Horng Wu,[2] Ming-Shien Yen, [1,*] Sing-You Lai[1]

1Department of Materials Engineering, Kun Shan University, Tainan 71003, Taiwan, ROC

2 Green Energy & Eco-Technology Center, Industrial Technology Research Institute, Tainan70955, Taiwan, ROC

Abstract

We report on the synthesis of novel zirconia/silica /thiazole azo dye hybrid materials by a sol–gel process with vinyltriethoxysilane (VTES) as a precursor. The materials were synthesized from zirconium n-propanoxide and tetraethoxysilane (TEOS) with thiazole azo dyes, which were synthesized using 2-amino thiazole as the coupling component and then underwent a coupling reaction with the diazonium component p-nitroaniline. Alternatively, the thiazole azo dyes were processed by the hydrolysis–condensation reaction with a constant ratio of VTES and zirconium n-propanoxide and TEOS in appropriate proportions under a catalyst. The structures of these hybrid materials were examined by Fourier transform infrared analysis, ^{29}Si nuclear magnetic resonance, X-ray diffraction, and energy-dispersive X-ray spectroscopy.

Keywords—*zirconia, silica, thiazole dyes, hybrid materials.*

I. INTRODUCTION

Multifunctionalism and intelligence are modern design goals that have affected the design of all objects, regardless of their size. Therefore, hybrid materials have become widespread. Compared with traditional materials, one vital characteristic of hybrid materials is their designability. In the past 20 years, material design has emerged and been abundantly realized in hybrid materials. Organic–inorganic hybrid materials contain both organic and inorganic functionality and provide functional compensation and optimization [1-5]. Consequently, they are widely used in numerous fields including optics, and catalysis, and in other biomaterials.

Zirconium dioxide (ZrO2) was developed recently and has been widely applied in thin films. ZrO2 features a high refractive index, ablation resistance, chemical stability, and dielectric, insulating, and mechanical properties [6-9]. It is also applied in thermal barrier coatings, insulation, abrasion-resistant coatings, and corrosion protection coatings, and in the manufacture of photoelectric components and electrochemical biosensors. It is frequently used in various industries, including aviation and aerospace, ferrous metallurgy, machine manufacture, and optics, and it possesses strong potential for other applications [10-13]. ZrO2 is a ceramic material with a crystal size of approximately 100 nm. The crystalline structure is dense and possesses low porosity, which provides a high coating layer binding capacity.

Furthermore, silica is a natural material derived from common materials such as quartz, sand, and flint. Silica has high chemical stability, a low thermal expansion coefficient, and high heat resistance. The relatively high chemical stability of the silica phase can be advantageous in some cases [14-17]. If zirconia and silica gels are sufficiently intermixed in the surface layer during the condensation polymerization process, a short travelling distance between the surface-modified silica thermal stability sites and the mechanical strength sites on the boehmite phase may result in high chemical stability.

The molecules of heteroaryl azo dyes contain unshared electron pairs of nitrogen and sulphur, which can easily trigger resonance and cause the π electrons of the compound to leap from the ground state to the excited state. The synthesis and spectroscopic properties of azo dyes are well-established [18-22]. The use of heterocyclic aromatic amines to improving the tinctorial strength has been well established. 2-Aminothiazole compounds which possess different substituents in the 4-position of the analogous derivatives as diazo components tend toward bathochromic shifts, unlike analogous dyes derived from benzenoid compounds [23-25].

Modern industries and consumers desire multifunctional products; therefore, multifunctioning organic–inorganic hybrid materials have become popular. The sol–gel method is a frequently used organic–inorganic hybrid material preparation method that combines inorganic and organic molecular networks [26-31]. Zirconium-containing oxide materials obtained by sol–gel synthesis that yielded a transparent solid gel are expected to find wide practical application. Zirconium n-propoxide (TPOZ) can be used to increase the functionality of hybrid materials. The use of the precursor TPOZ was

suggested to produce zirconia gel, which was subsequently incorporated in other organic material syntheses to create hybrid materials that are widely used to produce various chemical products. The zirconia network structure was combined with a siloxane network to increase the additive effect, thereby obtaining heat accumulation capability and superhydrophobicity. Subsequently, the sol–gel method was applied to prepare organic–inorganic hybrid dyes; it yielded hybrid materials exhibiting a network structure consisting of the processed dye, VTES/TPOZ, and VTES/TEOS/TPOZ through additive hydrolysis. This will enable the use of hybrid dyes when processing high molecular products.

II. EXPERIMENT

A. Analytical Instruments

Fourier-transform infrared (FT-IR) spectra were recorded on a Bio-Rad Digilab FTS-40 spectrometer (KBr); ^{1}H nuclear magnetic resonance (NMR) spectra were obtained on a BRUKER AVANCE 400MHz NMR spectrometer. Chemical shifts (δ) are expressed in parts per million using tetramethylsilane (TMS) as an internal standard. The ^{29}Si-NMR spectra were collected using a BRUKER **AVANCE 400** MHz NMR spectrometer at 78.49 MHz, with a recycle time of 60 s, and the number of scans was 914. The elemental analysis was carried out using a Philips XL40 FEG-Energy Dispersive X-ray Spectrometer. X-ray diffraction (XRD) measurements were performed on a Rigaka D/MAX 2500V X-ray powder diffractometer in steps of 0.01° using Cu K_α radiation as the X-ray source.

B. Materials

VTES, tetraethoxysilane (TEOS), TPOZ {$Zr[O(CH_2)_2CH_3]_4$}, acetophenone, and *p*-nitroaniline were purchased from Acros Co., Ltd., Belgium. Thiourea, sulphuric acid, and iodide were purchased from Hayashi Pure Chemical Co., Ltd.

C. Preparation of dye 5-[2-(4-nitrophenyl)-diazen-1-yl]-4-phenyl-1,3-thiazol- 2-amine (3)

A finely ground powder of *p*-nitroaniline **2** (1.38 g, 0.01 mol) was added to hydrochloric acid (12 mL) and stirred for 20 min. Sodium nitrite (0.72 g, 0.0105 mol) was added in portions to concentrated sulphuric acid (5 mL) at 10°C and stirred for 1 h at 60–65°C. The solution was cooled to below 5°C, and then the finely ground derivatives were slowly added; the mixture was stirred for an additional 1 h at 5–10°C until it was clear. The resulting diazonium solution was used immediately in the coupling reaction. A clear mixed solution of the coupling component 4-phenyl-2-aminothiazole **1** (2.0 g, 0.01 mol) and 10% sodium carbonate was stirred. The diazonium mixture was added at 0–5°C, and the solution was stirred for at least 2 h; it was diluted to raise its pH to 5–6 (by adding aqueous sodium hydroxide or sodium acetate). The resulting product

was filtered, washed with water, and re-crystallized from ethanol to give a deep red solid, 5-[2-(4-nitrophenyl)-diazen-1-yl]- 4-phenyl-1,3-thiazol-2-amine (**3**) (2.3 g, 70%). M.P. 245-247°C; Fourier transform infrared (FTIR) (KBr)/cm^{-1}: 3433 (NH_2), 3057 (C–H); ^{1}H NMR (DMSO-d_6) δ ppm: 7.04 (1H, s, –NH_2), 7.51–7.55 (5H, m, ArH), 7.71, (2H, d, 2,6-Ph–H), 8.19 (2H, d, 3,5- Ph–H). $C_{15}H_{17}N_2O_2S$ (325.1) Calcd.: C, 55.38; H, 3.41; N, 21.53; O, 9.84; S, 9.85. Found: C, 55.32; H, 3.44; N, 21.58; O, 9.78; S, 9.87.

D. Preparation of precursor 5-[2-(4-nitrophenyl)-diazen-1-yl]-4-phenyl-N-[2-(triethoxysilyl)ethyl]-1,3- thiazol-2-amine (4)

Precursor **4** was prepared by the reaction of dye **3** (3.25 g, 0.01 mol) followed by the addition of VTES (9.5 g, 0.05 mol) in ethanol (80 mL) with stirring at 65°C for 4 h at an adjusted pH of 4–5. The resulting product was filtered, washed with water, and re-crystallized from ethanol to give a dark red solid, 5-[2-(4-nitrophenyl)-diazen-1-yl]- 4-phenyl-N-[2-(triethoxysilyl)ethyl]-1,3-thiazol-2- amine (**4**) (2.76 g, 59%). M.P. 304–306°C; FTIR (KBr)/cm^{-1}: 3395 (NH), 3073 (C–H), 1096 (O–Si). $C_{23}H_{29}N_5O_5SSi$ (515.4) Calcd.: C, 53.57; H, 5.67; N, 13.58; O, 15.51; S, 6.22; Si, 5.45. Found: C, 53.63; H, 5.62; N, 13.56; O, 15.55; S, 6.28; Si, 5.41.

E. Preparation of Zirconia Gel

We prepared zirconia gel by dissolving TPOZ and ethanol at a 1:30 molar ratio and hydrolysed the TPOZ in water at a 1:4 molar ratio. The mixture was heated under reflux for 30 min until completely dissolved; the pH value was adjusted to approximately 3–4 using nitric acid, and the mixture was then stirred until it became clear.

F. Synthesis of Hybrid Materials 5, 6

As shown in Scheme 1, precursor **4** and zirconia gel were mixed according to a fixed ratio; 0.01 mol of hydrochloric acid and 10 mL of water were added to maintain a pH level of 3–4, and the mixture was placed in a thermostat stirrer and heated under reflux for 4 h to produce a condensation reaction and the hybrid material. We altered the concentration of zirconia gel to produce varying degrees of polycondensation reaction and obtained hybrid materials **5** and **6**.

G. Preparation of hybrid materials Z1–Z4, D1–D4, and F1–F4

Hybrid material Z_1 was prepared by condensation of precursor 4 (5.01 g, 0.01 mol) and zirconia sol (0.01 mol) in ethanol (80 mL) by stirring at 65°C for 2 h, by adding hydro-
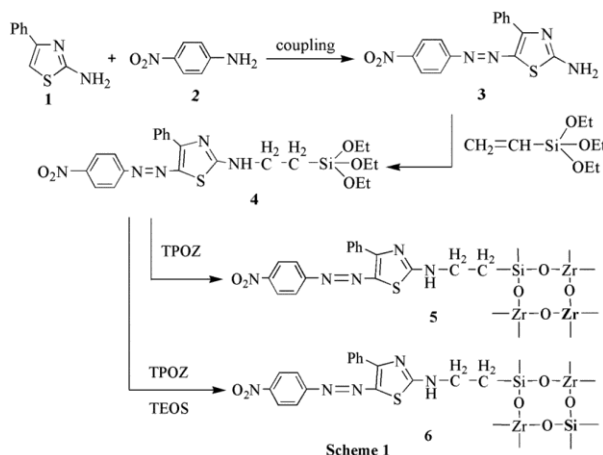
Scheme 1 Synthesis of Hybrid Material 5, 6

chloric acid (0.365 g, 0.01 mol) and water (5 mL). Hybrid materials Z_2–Z_4 were synthesized using the same method as that used for synthesizing Z_1. Hybrid materials Z_1–Z_4 were prepared using different molar ratios of precursor 4 to the zirconia sol in hydrolysis polycondensation; the molar ratios were 1:1, 1:1.5, 1:2, and 1:3, respectively. Hybrid material D_1 was prepared by condensation of precursor 4 (5.01 g, 0.01 mol), TEOS (4.16 g, 0.01 mol), and zirconia sol (0.02 mol) in ethanol (80 mL) by stirring at 65°C for 2 h, by adding hydrochloric acid (0.365 g, 0.01 mol) and water (5 mL). Hybrid materials D_2–D_4 were synthesized using the same method as that used for synthesizing D_1. Hybrid materials D_1–D_4 were prepared using different molar ratios of precursor 4 to TEOS and the zirconia sol in hydrolysis polycondensation at a constant ratio of the zirconia sol; the molar ratios were 1:1:2, 1:1.5:2, 1:2:2, and 1:3:2, respectively. Hybrid material F_1 was prepared by condensation of precursor 4 (5.01 g, 0.01 mol), TEOS (4.16 g, 0.02 mol), and the zirconia sol (0.01 mol) in ethanol (80 mL) by stirring at 65°C for 2 h, by adding hydrochloric acid (0.365 g, 0.01 mol) and water (5 mL). Hybrid materials F_2–F_4 were synthesized using the same method as that used for synthesizing F_1. Hybrid materials F_1–F_4 were prepared using different molar ratios of precursor 4 to TEOS and the zirconia sol in hydrolysis polycondensation at a constant ratio of TEOS; the molar ratios were 1:2:1, 1:2:1.5, 1:2:2, and 1:2:3, respectively.

III. RESULTS AND DISCUSSION

A. FTIR Analysis

Figures 1 and 2 show the FTIR spectra of Z_1–Z_4 and D_1–D_4, respectively. The absorption peaks of the N–H and C–H functional groups were observed at approximately 3440 and 3113 cm^{-1}, respectively. In the FTIR spectra of precursor 4, there is an obvious deviation of the amino group absorption peaks close to 3419 cm^{-1} and the absorption peaks around 3395 cm^{-1}, revealing that some of the dye reacted with VTES [32]. Figure 1 shows that hybrid materials Z_1–

Z_4 exhibited a characteristic zirconia peak at approximately 466 cm^{-1}, increased the zirconia gel proportion, and a substantially enhanced Zr–O absorption peak. In addition, an Si–O absorption peak appeared at approximately 1098 cm^{-1}, and a characteristic Zr–O–Si peak appeared from approximately 800 to 1100 cm^{-1}. After additional zirconia gel was added, the peak absorption strength weakened for the Z_1 sample. A Si–C absorption peak appeared at approximately 1243 cm^{-1}. Further, a peak characteristic of the benzene functional group appeared from approximately 1615 to 1590 cm^{-1}, and absorption peaks corresponding to the N–H and C–H functional groups appeared at approximately 2934 and 2962 cm^{-1}, respectively. Nitric acid consumption also increased with increasing amount of zirconia gel, causing the N–H and C–H functional group absorption peaks to shift leftward. The results presented in Figure 2 indicate that when the amount of zirconia gel was fixed, hybrids D_1–D_4 showed no significant differences in the Zr–O functional group characteristic peak at 466 cm^{-1}, although the intensity of the Si–O absorption peak was enhanced substantially by increasing the TEOS proportion. The absorption peak ranges for D_1–D_4 were the same as those for Z_1–Z4. The results were then compared with that for Z_3 (Figure 1) to identify why a significant difference was not observed. It was found that when the ZrO_2 proportion was fixed, the consumption of nitric acid increased, shifting the characteristic peak leftward. The results presented in Figure 3 indicate that hybrids F_1–F_4 exhibited a characteristic peak for the Zr–O functional group at 466 cm^{-1}, which increased substantially with increasing zirconia proportion.
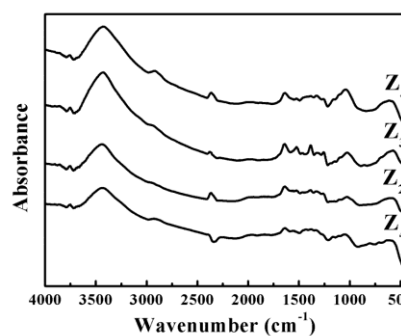
Fig. 1 FT-IR Spectra of Hybrid Materials Z_1–Z_4
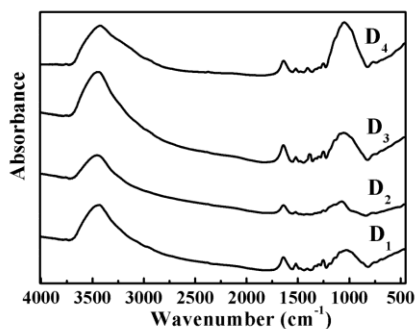
Fig. 2 FT-IR Spectra of Hybrid Materials D_1–D_4
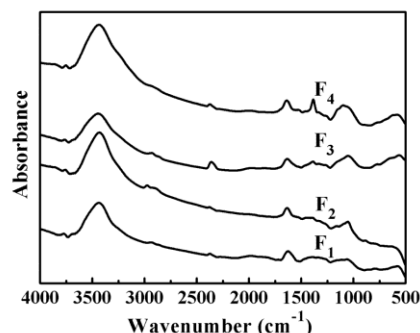
Fig. 3 FT-IR Spectra of Hybrid Materials F_1–F_4

The absorption peak ranges were similar to those shown in Figure 1: Si–O was observed at approximately 1098 cm^{-1}, the characteristic peak of the Zr–O–Si functional group appeared from 800 to 1100 cm^{-1}, the characteristic peak of the benzene functional group appeared from 1615 to 1590 cm^{-1}, and the N–H and C–H functional groups appeared at 2934 and 2962 cm^{-1}, respectively.

B. ^{29}Si NMR spectra analysis

^{29}Si NMR [33] is often used to characterize the structures formed by Si hydrolysis. While the FTIR results above indicated the formation of Si–O–Si bonds by a sol–gel reaction, solid-state ^{29}Si NMR provided additional information on the structure of the silica and the extent of the Si–OH condensation reaction. The T^3, Q^3, and Q^4 absorption peaks were located by applying ^{29}Si NMR spectroscopy. Figure 4 shows that the ^{29}Si NMR spectra of the simple dye and VTES contain absorption peaks at ~69.56 ppm (T^2) and ~80.71 ppm (T^3), corresponding to Si–OR formation following the hydrolysis of VTES. Figure 5 shows the ^{29}Si NMR spectra of the processed hybrid dye formed with various proportions of VTES and TEOS. Peaks appear at ~101.06 ppm (Q^3) owing to absorption by (H–O)Si(-OSi≡)$_3$ structures and at ~108.91 ppm (Q^4) owing to absorption by Si(–OSi≡)$_4$ structures. The structure of the Si–OR absorption peak indicated that some Si quadruple bonds had an unreacted Si–OH functional group, (H–O)Si(–OSi ≡)$_3$ and some Q^3 quadruple bonds had an unreacted

Si–O functional group, Si(–OSi≡)$_3$. The structure of Q^4 indicates that the Si quadruple bond reacted completely with the Si–O functional group: Si(-OSi≡)$_4$.

No irregular peak was observed in Figure 5 for hybrids D_1–D_4 with a fixed zirconia proportion, varying TEOS proportions, and an increased hybrid material proportion. The T^3 and Q^3 absorption peaks were observed; however, the noise peaks were greater, and only the T^3 absorption peak was observed when the smallest amount of TEOS was added. In the spectrum of hybrid D_2, the strength of the Q^3 absorption peak (at approximately 100.52 ppm) increased, and the Q^4 absorption peak appeared at a δ value of ~109.13 ppm. In addition, the T^3 absorption peak was diminished and no longer exhibited a noise peak. The results for hybrid **D_3** indicated that double absorption peaks disappeared and were replaced by a single Q^3 absorption peak at a δ value of ~98.44 ppm; the Q^4 absorption peak increased, and the T^3 absorption peak decreased significantly. Regarding hybrid **D_4**, the Q^4 absorption intensity increased substantially, and the T^3 absorption intensity decreased. The Q^4 absorption peak for hybrids **D_2–D_4** gradually shifted into a Q^3 absorption peak, as shown in Figure 5. Therefore, with increasing TEOS proportion, Si–O replaced Zr–O, and Si–O–Zr was formed. The noise peak reduction indicated that increasing the TEOS proportion enhanced the network structure purity.

Spectral analysis of hybrid Z_3 (Figure 4) indicated that when zirconia alone was condensation polymerised with
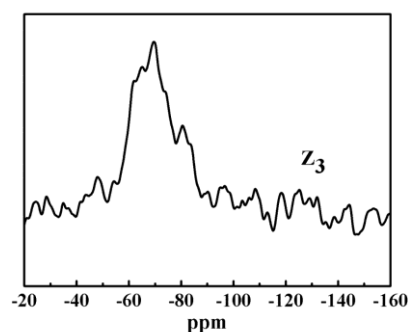
Fig. 4 ^{29}Si-NMR Spectra of Hybrid Material Z_3
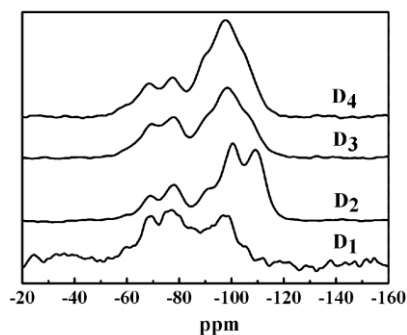
Fig. 5 ^{29}Si-NMR Spectra of Hybrid Materials D$_1$–D$_4$

VTES, the network structure purity was reduced, causing numerous noise peaks. Therefore, although the addition of zirconia formed the Zr–O–Zr bond network structure, the absorption peak of VTES in T^3 appeared at δ value of ~69.56 ppm, which indicated that adding only zirconia could not eliminate the noise peaks.

C. Energy-Dispersive X-Ray Spectra Analysis

The energy-dispersive X-ray spectroscopy (EDS) analysis results are presented in Table 1 and Figure 6. When additional zirconia gel was added to hybrids Z$_1$–Z$_4$, the quantity of zirconium increased, which caused the quantity of Si to decrease. It is possible that the carbon proportion decreased and the oxygen increased in the hybrid material because of the formation of additional Zr–O–Zr bonds in zirconia thin films of hybrids Z$_1$–Z$_4$ and the gradually increasing zirconium proportion.
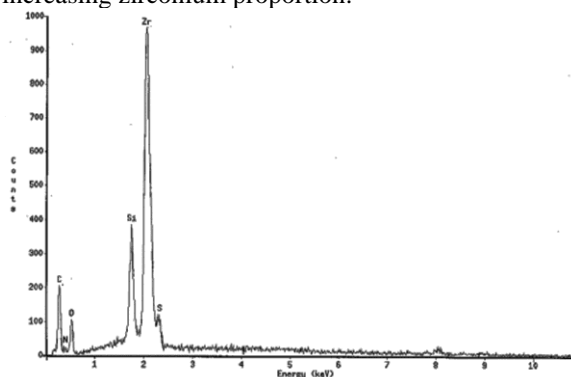
Fig. 6 The EDS Diagram of Hybrid Materials Z$_3$

Table 1: EDS Analysis of Hybrid Materials Z$_1$–Z$_4$, D$_1$–D$_4$, and F$_1$–F$_4$

Samples	Elemental composition (%)					
	C	O	Si	N	Zr	S
Z$_1$	32.13	13.52	7.56	5.96	38.29	2.54
Z$_2$	34.36	13.75	4.62	5.95	40.10	1.22
Z$_3$	28.31	14.20	4.45	6.62	44.20	2.22
Z$_4$	21.84	13.47	6.43	6.53	50.34	1.39
D$_1$	22.79	24.33	15.38	5.38	30.14	1.98
D$_2$	25.34	21.23	17.25	3.51	30.74	1.93
D$_3$	18.22	22.26	22.08	4.44	31.16	1.84
D$_4$	16.98	19.03	25.68	3.30	32.52	2.49
F$_1$	32.28	21.71	19.63	3.96	20.45	1.97
F$_2$	27.16	17.02	19.32	4.33	30.24	1.93
F$_3$	21.36	20.50	22.00	3.57	30.25	2.32
F$_4$	20.65	24.06	21.02	4.14	28.70	1.43
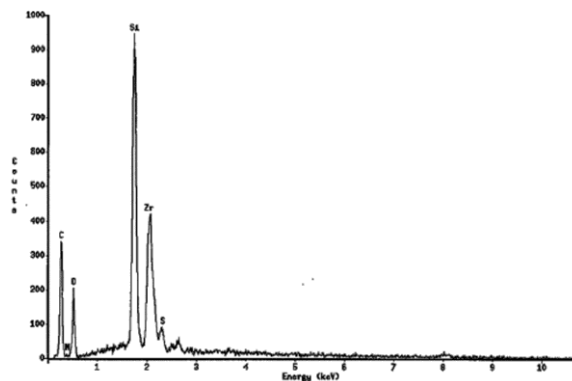
Fig. 7 The EDS Diagram of Hybrid Materials D$_3$
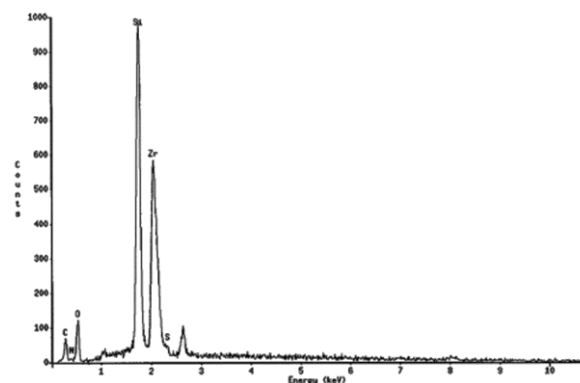
Fig. 8 The EDS Diagram of Hybrid Materials F$_3$

As shown in Table 1 and Figure 7, hybrids D$_1$–D$_4$ had a fixed molar concentration of zirconia gel and a moderately increasing molar concentration of TEOS. The EDS analysis results indicated that the increase in the Si level when the TEOS content increased could be explained by the formation of a zirconia thin film with Zr–O–Zr bonds and the replacement of Zr with Si. Table 1 shows that when the TEOS proportion was fixed in hybrids **F$_1$–F$_4$**, the amount of Si decreased with increasing zirconia content. Similar results were observed for hybrids D$_1$–D$_4$: Si was steadily replaced with Zr in the Zr–O–Si bonds in the thin film, as shown in Figure 8.

D. X-Ray Diffraction Analysis

In this study, we performed an X-ray diffraction analysis of hybrid materials in the Z, D, and F series with various proportions and unsintered Zr powder developed by a sol–gel process (hereafter, Zr powder). Because neither the series of hybrid materials nor the Zr powder was sintered, all of these materials exhibited amorphous structures without clear crystal phase peaks, as shown in Figures 9 and 10. Figure 9 shows that the diffraction peaks of F$_1$, F$_2$, F$_3$, and F$_4$ occur at 2θ = 25°, 26°, 26°, and 27°,

respectively.Figure 10 shows that the diffraction peaks of the Zr powder, inoculated Zr-series hybrid material Z_4, hybrid material D_4, and hybrid material F_4 appear at $2\theta = 31°$, $27°$, $24°$, and $27°$, respectively. These results indicate that with the exception of the Zr powder, the morphology of amorphous-phase VTES and TEOS affected the diffraction peaks of the hybrid materials Z_4, D_4, and F_4, producing slight shifts to the left.
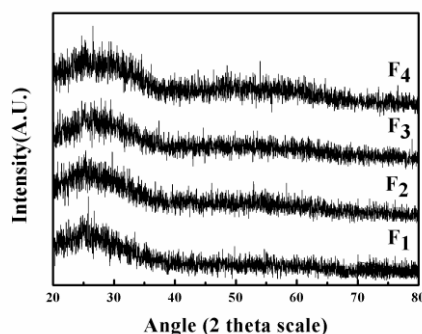
Fig. 9 The XRD Diagram of Hybrid Materials F_1–F_4
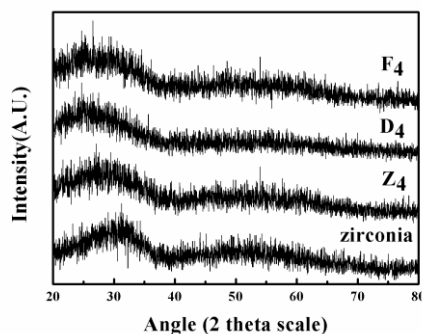
Fig. 10 The XRD Diagram of Hybrid Materials Z_4, D_4, and F_4

IV. CONCLUSIONS

This study focused primarily on synthesis of a series of heterocyclic thiazole dyes with various proportions of added VTES/TPOZ and VTES/TEOS/TPOZ using the sol–gel method. The derived hybrids were further analysed to understand their chemical and physical properties. FTIR analysis showed that the absorption peak of the Zr–O functional group appeared at 466 cm^{-1} and the characteristic peak of the Zr–O–Si functional group appeared from 800 to 1100 cm^{-1}, verifying the network structure. The ^{29}Si NMR analysis results indicated that the peak of hybrids D_1–D_4 increased as the TPOZ ratio increased. This reduced the T^3 absorption peak (which represented the increase in Si–O–Si) and caused Q^4 to steadily shift toward Q^3. These results indicated that Si–O–Si was gradually transformed into Zr–O–Si, and the presence of Si–O–Si and Zr–O–Si was observed. The EDS results showed that when additional zirconia gel was added to hybrids Z_1-Z_4, the zirconia level rose, causing the

Si level to continuously decrease. The diffraction peak of the Zr powder, inoculated Zr-series hybrid material Z_4, hybrid material D_4, and hybrid material F_4 appeared at $2\theta = 31°$, $27°$, $24°$, and $27°$, respectively.

REFERENCES

[1] F. Hoffmann, M. Cornelius, J. Morell, and M. Fröba, "Silica-based mesoporous organic–inorganic hybrid materials," Angew. Chem. Int. Ed., vol. 45, pp. 3216–3251, May. 2006.

[2] C. Sanchez, B. Julián, P. Belleville, and M. Popall, "Applications of hybrid organic–inorganic nanocomposites," J. Mater. Chem., vol. 15, pp. 3559–3592, Aug. 2005.

[3] P. Judeinstein, and C. Sanchez, "Hybrid organic–inorganic materials a land of multidisciplinarity," J. Mater. Chem., vol. 6(4), pp. 511–525, Apr. 1996.

[4] Y. H. Han, A. Taylor, M. D. Mantle, and K. M. Knowles, "Sol–gel-derived organic–inorganic hybrid materials," J. Non-Cryst. Solids., vol. 353, pp. 313–320, Mar. 2007.

[5] R. D. Maggio, S. Dirè, E. Callone, F. Girardi, and G. Kickelbick, "Hybrid organic–inorganic materials using zirconium based NBBs and vinyl trimethoxysilane: Effect of pre-hydrolysis of silane," Polymer, vol. 51, pp. 832–841, Jan. 2010.

[6] G. Cheng. "An inorganic–organic hybrid precursor strategy for the synthesis of zirconium diboride powders," Int. J. Refract. Met. Hard Mater., vol. 36, pp.149–153, Aug. 2013.

[7] J. Zhao, W. Fan, D. Wu, and Y. Sun, "Synthesis of highly stabilized zirconia sols from zirconium,"J. Non-Cryst. Solids, vol. 261, pp. 15–12, Jan. 2000.

[8] K. Joy, S. S. Lakshmy, P. B. Nair, and G. P. Daniel, "Band gap and superior refractive index tailoring properties in nanocomposite thin film achieved through sol–gel co-deposition method," J. Alloys Compd., vol. 512, pp. 149–155, Oct. 2012.

[9] E. L. Corral, and L. S. Walker, "Improved ablation resistance of C–C composites using zirconium diboride and boron carbide," J. Eur. Ceram. Soc., vol. 30, pp. 2357–2364, Apr. 2010.

[10] P. C. R. Varma, J. Colreavy, J. Cassidy, M. Oubaha, C. McDonagh, and B. Duffy, "Corrosion protection of AA 2024-T3 aluminium alloys using 3, 4-diaminobenzoic acid," Thin Solid Films, vol. 518, pp. 5753–5761, May. 2010.

[11] S. Jesurani, S. Kanagesan, M. Hashim, and I. Ismail, "Dielectric properties of Zr doped $CaCu_3Ti_4O_{12}$ synthesized by sol–gel route," J. Alloys Compd., vol. 551, pp. 456–462, Nov. 2013.

[12] J. Dong, Y. Wen, Y. Miao, Z. Xie, Z. Zhang, and H. Yang, "A nanoporous zirconium phytate film for immobilization of redox protein and the direct electrochemical biosensor," Sens. Actuators, B, vol. 150, pp. 141–147, Aug. 2010.

[13] P. K. Q. Nguyen, and S. K. Lunsford, "Electrochemical response of carbon paste electrode modified with mixture of titanium dioxide zirconium dioxide in the detection of heavy metals lead and cadmium," Talanta, vol. 101, pp.110–121, Sep. 2012.

[14] W. Zhou, J. E. Mark, M. R. Unroe, and F. E. Arnold, "Toughening of a high-temperature polymer by the sol–gel, in situ generation of a rubbery silica–siloxane phase," J. Appl. Polym. Sci., vol. 79, pp. 2326–2330, Jun. 2001.

[15] N. D. Hegde, and A. V. Rao, "Physical properties of methyltri-methoxysilane based elastic silica aerogels

prepared by the two-stage sol–gel process," J. Mater. Sci., vol. 42, pp. 6965–6971, Apr. 2007.

[16] Y. Dimitriev, Y. Ivanova, and R. Iordanova," History of sol–gel science and technology," J. Univ. Chem. Technol. Metall., vol. 43(2), pp. 181–192, May. 2008.

[17] X. Du, and J. He, "A self-templated etching route to surface-rough silica nanoparticles for superhydrophobic coatings," ACS Appl. Mater. Interfaces, vol. 3, pp. 1269–1276, Mar. 2011.

[18] I. Zadrożna, and E. Kaczorowska, "Synthesis and absorption spectra of hetarylazo dyes derived from coupler 4-aryl-3-cyano-2-aminothiophenes," Dyes Pigm., vol. 71, pp. 207–211, Oct. 2006.

[19] A. D. Towns, "Developments in azo disperse dyes derived from heterocyclic diazo components," Dyes Pigm., vol. 42, pp. 3–28, Nov. 1999.

[20] G. Hallas, and A. D. Towns, "A comparison of the properties of some 2-aminothiophene-derived disperse dyes," Dyes Pigm., vol. 31, pp. 273–289, Dec. 1996.

[21] I. Zadrożna, and E. Kaczorowska, "Synthesis and characteristics of azo chromophores for nonlinear-optical application," Dyes Pigm., vol. 71, pp. 207–211, Sep. 2006.

[22] M. S. Yen, and I. J. Wang, "A facile syntheses and absorption characteristics of some monoazo dyes in bis-heterocyclic aromatic systems part II: syntheses of 4-(p-substituted) phenyl-2- (2-pyrido-5-yl and 5-pyrazolo-4-yl) azo-thiazole derivatives," Dyes Pigm., vol. 63, pp. 1–9, Dec. 2004.

[23] G. Hallas, and J. H. Choi, "Synthesis and spectral properties of azo dyes derived from 2-aminothiophenes and 2-aminothiazoles,"Dyes Pigm., vol. 42, pp. 249–265, Feb. 1999.

[24] A. T. Peters, and S. S. Yang, "Monoazo disperse dyes derived from nitro-2-aminobenzothiazoles," Dyes Pigm., vol. 28, pp. 151–164, Feb. 1995.

[25] A. T. Peters, and S. S. Yang, "Monoazo disperse dyes derived from mononitro-dichloro-2-aminobenzothiazoles," Dyes Pigm., vol. 30, pp. 291–299, Jul. 1996.

[26] N. Petkova, S. Dlugocz, and S. Gutzov, "Preparation and optical properties of transparent zirconia sol–gel materials," J. Non-Cryst. Solids, vol. 357, pp. 1547–1551, Mar. 2011.

[27] D. A. Ward, and E. I. Ko, "Use of preformed sols in the sol–gel preparation of zirconia," Langmuir, vol. 11, pp. 369–372, Sep. 1996.

[28] Sowntharya, L., Gundakaram, R. C., Raju, K. R. C. S., and R. Subasri, "Effect of addition of surface modified nanosilica into silica–zirconia hybrid sol–gel matrix," Ceram. Int., vol. 39, pp. 4245–4252, Nov. 2013.

[29] M. A. Wahab, and H. Chaobin, "Hydrogen–bond directed self–organized lamellar nanostructured benzene bridged- polysilsesquioxane free- standing monolithic structures via sol–gel method," Soft Mater., vol. 7(2), pp. 79–92, Jun. 2009.

[30] Z. Zhan, and H. C. Zeng, "A catalyst-free approach for sol–gel synthesis of highly mixed ZrO_2–SiO_2 oxides," J. Non-Cryst. Solids, vol. 243, pp. 26–38, Jan. 1999.

[31] S. Pandey, and S. B. Mishra, "Sol–gel derived organic–inorganic hybrid materials synthesis, characterizations and applications," J. Sol-Gel Sci. Technol., vol. 59, pp. 73–94, Apr. 2011.

[32] M. S. Yen, and M. C. Kuo, "Sol–gel synthesis of organic-inorganic hybrid materials comprising boehmite, silica, and thiazole dye," Dyes Pigm., vol. 94(2), pp. 349–354, Aug. 2012.

[33] R. J. Hook, "A ^{29}Si-NMR study of the sol–gel polymerisation rates of substituted ethoxysilanes," J. Non-Cryst. Solids, vol. 195, pp. 1–15, Feb. 1996.